ESC European Society of Cardiology

European Heart Journal (2021) **42**, 4847–4861
doi:10.1093/eurheartj/ehab660

TRANSLATIONAL RESEARCH
Dyslipidaemias

Macrophage NFATc3 prevents foam cell formation and atherosclerosis: evidence and mechanisms

Xiu Liu [1,2,†], Jia-Wei Guo[2,3,†], Xiao-Chun Lin [2,†], Yong-Hua Tuo[4,†], Wan-Li Peng[2,†], Su-Yue He[5], Zhao-Qiang Li[6], Yan-Chen Ye [7,8], Jie Yu[9], Fei-Ran Zhang[1,2], Ming-Ming Ma[2], Jin-Yan Shang[2], Xiao-Fei Lv[2], An-Dong Zhou[10], Ying Ouyang[11], Cheng Wang[1], Rui-Ping Pang[5], Jian-Xin Sun[12], Jing-Song Ou[8,13,*], Jia-Guo Zhou[1,2,14,15,16,*], and Si-Jia Liang [1,2,*]

[1]Program of Kidney and Cardiovascular Diseases, the Fifth Affiliated Hospital, Zhongshan School of Medicine, Sun Yat-Sen University, 74 Zhongshan 2 Rd, Guangzhou 510080, China; [2]Department of Pharmacology, Cardiac and Cerebral Vascular Research Center, Zhongshan School of Medicine, Sun Yat-Sen University, 74 Zhongshan 2 Rd, Guangzhou 510080, China; [3]Department of Pharmacology, School of Medicine, Yangtze University, 1 Nanhuan Rd, Jingzhou 434023, China; [4]Department of Neurosurgery, the Second Affiliated Hospital of Guangzhou Medical University, 250 Changgang East Rd, Guangzhou 510260, China; [5]Department of Physiology, Pain Research Center, Zhongshan School of Medicine, Sun Yat-Sen University, 74 Zhongshan 2 Rd, Guangzhou 510080, China; [6]Guangdong Provincial Key Laboratory of Tumor Immunotherapy, Cancer Research Institute, Southern Medical University, 1023 Shatai South Rd, Guangzhou 510515, China; [7]Division of Vascular Surgery, the First Affiliated Hospital, Sun Yat-Sen University, 58 Zhongshan 2 Rd, Guangzhou 510080, China; [8]National-Guangdong Joint Engineering Laboratory for Diagnosis and Treatment of Vascular Diseases, the First Affiliated Hospital, Sun Yat-Sen University, 58 Zhongshan 2 Rd, Guangzhou 510080, China; [9]Department of General Surgery, Zhujiang Hospital, Southern Medical University, 253 Industrial Rd, Guangzhou 510282, China; [10]Department of Clinical Medicine, the Second Clinical Medical School, Guangdong Medical University, 1 Xincheng Rd, Dongguan 523808, China; [11]Department of Pediatrics, Sun Yat-Sen Memorial Hospital, Sun Yat-Sen University, 107 Yanjiang West Rd, Guangzhou 510120, China; [12]Center for Translational Medicine, Thomas Jefferson University, 1020 Locust St., Rm. 368G, Philadelphia PA 19107, USA; [13]Division of Cardiac Surgery, Heart Center, the First Affiliated Hospital, Sun Yat-Sen University, 58 ZhongShan 2 Rd, Guangzhou 510080, China; [14]Department of Cardiology, Sun Yat-Sen Memorial Hospital, Sun Yat-Sen University, 107 Yanjiang West Rd, Guangzhou 510120, China; [15]Guangdong Province Key Laboratory of Brain Function and Disease, Zhongshan School of Medicine, Sun Yat-Sen University, 74 Zhongshan 2 Rd, Guangzhou 510080, China; and [16]Key Laboratory of Cardiovascular diseases, School of Basic Medical Sciences, Guangzhou Medical University, 1 Xinzao Rd, Guangzhou 511436, China

Received 7 February 2021; revised 13 June 2021; editorial decision 2 September 2021; accepted 2 September 2021; online publish-ahead-of-print 27 September 2021

See page 4862 for the editorial comment for this article 'Two birds, one stone: NFATc3 controls dual actions of miR-204 in foam cell formation', by C. Solingen and K.J. Moore, https://doi.org/10.1093/eurheartj/ehab640.

Aims Our previous study demonstrated that Ca^{2+} influx through the Orai1 store-operated Ca^{2+} channel in macrophages contributes to foam cell formation and atherosclerosis via the calcineurin–ASK1 pathway, not the classical calcineurin–nuclear factor of activated T-cell (NFAT) pathway. Moreover, up-regulation of NFATc3 in macrophages inhibits foam cell formation, suggesting that macrophage NFATc3 is a negative regulator of atherogenesis. Hence, this study investigated the precise role of macrophage NFATc3 in atherogenesis.

Methods and results Macrophage-specific NFATc3 knockout mice were generated to determine the effect of NFATc3 on atherosclerosis in a mouse model of adeno-associated virus-mutant *PCSK9*-induced atherosclerosis. NFATc3 expression was decreased in macrophages within human and mouse atherosclerotic lesions. Moreover, NFATc3 levels in peripheral blood mononuclear cells from atherosclerotic patients were negatively associated with plaque instability. Furthermore, macrophage-specific ablation of NFATc3 in mice led to the atherosclerotic plaque formation, whereas macrophage-specific NFATc3 transgenic mice exhibited the opposite phenotype. NFATc3 deficiency in macrophages promoted foam cell formation by potentiating SR-A- and CD36-meditated lipid uptake. NFATc3 directly targeted and transcriptionally up-regulated miR-204 levels. Mature miR-204-5p suppressed SR-A expression via canonical regulation. Unexpectedly, miR-204-3p localized in the nucleus and

* Corresponding authors. Tel: +86 20 87331857, Fax: +86 20 87331209, Email: liangsj5@mail.sysu.edu.cn (S.-J.L.); Tel: +86 20 87331857, Fax: +86 20 87331209, Email: zhoujg@mail.sysu.edu.cn (J.-G.Z.); Tel: +86 20 87331857, Fax: +86 20 87331209, Email: oujs@mail.sysu.edu.cn (J.-S.O.)
† These authors contributed equally to the study.

inhibited CD36 transcription. Restoration of miR-204 abolished the proatherogenic phenotype observed in the macrophage-specific NFATc3 knockout mice, and blockade of miR-204 function reversed the beneficial effects of NFATc3 in macrophages.

Conclusion Macrophage NFATc3 up-regulates miR-204 to reduce SR-A and CD36 levels, thereby preventing foam cell formation and atherosclerosis, indicating that the NFATc3/miR-204 axis may be a potential therapeutic target against atherosclerosis.

Graphical Abstract

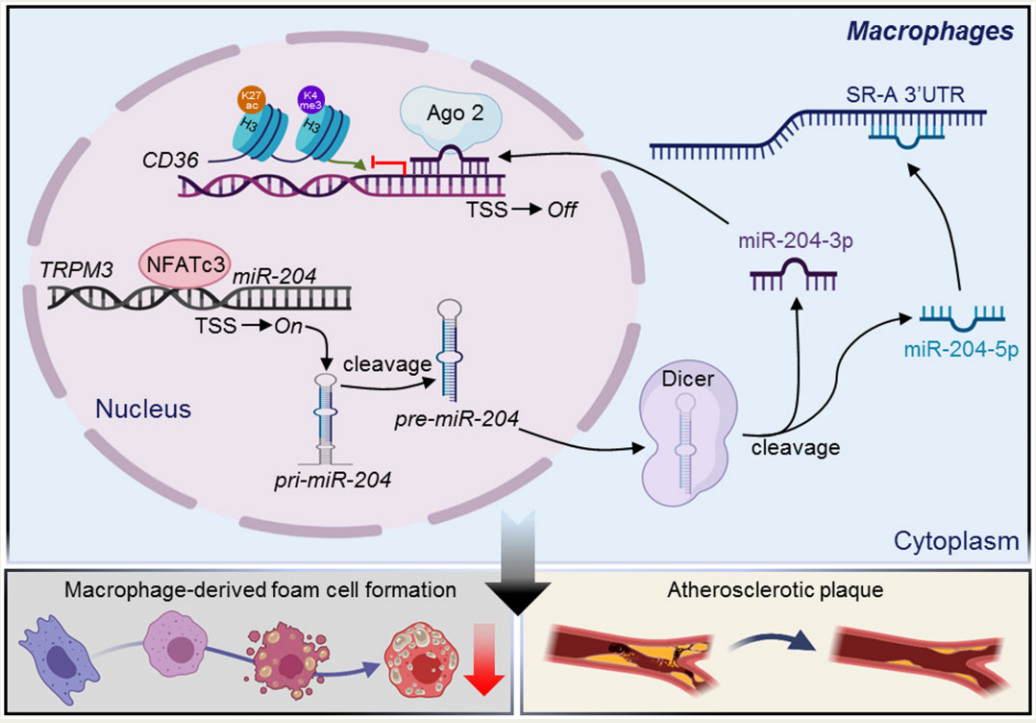

Macrophage NFATc3 inhibits foam cell formation and atherosclerosis via the cytoplasmic miR-204-5p/SR-A and nuclear miR-204-3p/CD36 axes.

Keywords Atherosclerosis • Macrophages • NFATc3 • MiR-204 • Scavenger receptors

Translational Perspective

Here, we show that NFATc3 levels in circulating peripheral blood mononuclear cells are negatively associated with disease severity in patients with atherosclerosis. Macrophage-specific knockout of NFATc3 promotes foam cell formation and atherosclerosis development in mice. Mechanistically, miR-204 is the direct target of NFATc3 and relays the inhibitory effects of NFATc3 on atherosclerosis. This study provides the first evidence that macrophage NFATc3 is an essential inhibitor of atherogenesis, suggesting that the NFATc3/miR-204 axis is a promising therapeutic target for atherosclerosis treatment. Furthermore, our results suggest that inhibition of calcineurin/NFAT signalling may underlie the proatherogenic effects of cyclosporine A and FK506.

Introduction

Atherosclerosis is a chronic progressive inflammatory disease involving the synergistic interaction of lipid metabolic factors with the cellular components of the vessels.[1,2] Formation of macrophage-derived foam cells is the hallmark of atherosclerosis.[1,3] During atherogenesis, monocytes are differentiated into macrophages in the subendothelial space and internalize oxidized low-density lipoproteins (oxLDL) through scavenger receptors such as SR-A and CD36.[4] The interplay between the scavenger receptors and oxLDL in macrophages induces the secretion of cytokines that recruits immune cells into the vascular wall. Increased uptake of oxLDL and/or reduced cholesterol efflux leads to lipid dysregulation in macrophages and promotes foam cell formation, triggering a series of inflammatory responses, ultimately establishing plaque formation and atherosclerotic lesions.[3] The importance of cholesterol-laden foam cells in atherogenesis together

with their enrichment within the plaques makes macrophages as a promising therapeutic target in atherosclerosis.[4]

The nuclear factor of activated T-cell (NFAT) family proteins was first identified as the transcription factors activated by the Ca^{2+}/calcineurin signalling in T cells.[5] NFATs consist of four well-characterized members (NFATc1–c4).[5] Because NFATs play critical roles in regulating the cytokine expression in T cells, the drugs that block the calcineurin/NFAT signalling, including cyclosporine A and FK506, have been widely used as immunosuppressive agents in organ transplant patients.[6–8] Meanwhile, it has been increasingly recognized that NFATs also play various roles outside the immune system.[9,10] Several studies have shown that NFATs function as important regulators of genes implicated in cardiovascular diseases, such as atherosclerosis.[11–13] However, individual NFAT isoforms exhibit different effects on cardiovascular diseases.[9,10,13] A better understanding of the roles of NFAT signalling in the cardiovascular system may help develop new therapeutic strategies for cardiovascular diseases.

Notably, clinical monitoring of the transplant patients with cyclosporine A or FK506 therapy has revealed that cardiovascular diseases, particularly atherosclerosis, are widespread and the most common cause of mortality among these patients, surpassing even infections.[14,15] The mechanisms underlying these adverse effects are assumed to be associated with metabolic, inflammatory, and coagulatory disorders.[7,14,16] Whether the blockade of calcineurin/NFAT is directly involved in these adverse effects is still a mystery. Recently, we reported that the hyperlipidaemia-induced Ca^{2+} influx in macrophages via Orai1 store-operated Ca^{2+} channel contributes to the foam cell formation and atherosclerosis.[17] The increase in intracellular Ca^{2+} concentration ($[Ca^{2+}]_i$) promotes atherosclerosis by activating calcineurin/ASK1signalling, but not calcineurin/NFATc3 signalling. Furthermore, overexpression of NFATc3 in macrophages has been shown to inhibit foam cell formation.[17] Together, these data indicate that the activation of NFATc3 in macrophages may prevent atherogenesis. However, the exact functions of macrophage NFATc3 signalling during atherogenesis have not yet been elucidated.

This study aims to investigate the functional significance of macrophage NFATc3 in atherosclerosis. The results demonstrated that NFATc3 expression is reduced in peripheral blood mononuclear cells (PBMCs) and plaques of atherosclerotic patients. Macrophage-specific knockout of NFATc3 potentiates atherosclerotic lesion formation, whereas macrophage NFATc3 prevents atherogenesis by down-regulating the scavenger receptors SR-A and CD36 via miR-204 axis.

Methods

Materials and methods are available in the Supplementary material online.

Results

Down-regulation of NFATc3 in macrophages during atherogenesis

We found that NFATc3 is a predominant isoform and highly expressed in human monocyte-derived macrophages (HMDMs) and mouse bone marrow-derived macrophages (BMDMs) (Supplementary material online, *Figure S1A and B*). In the plaques of carotid arteries from atherosclerosis patients, the nuclear accumulation of NFATc3 in macrophages was reduced, compared with in those from healthy controls (*Figure 1A*). Reduced nuclear accumulation of NFATc3 in macrophages was also observed in the atherosclerotic lesions of *Apoe*$^{-/-}$ mice fed a high-fat diet (HFD) (*Figure 1B*) and in HMDMs and mouse BMDMs treated with oxLDL (*Figure 1C and D*). However, oxLDL treatment barely affected the distribution of NFATc1, NFATc2, and NFATc4 in BMDMs (Supplementary material online, *Figure S1C–E*). Furthermore, oxLDL treatment reduced NFATc3 mRNA levels in both the nuclear and cytoplasmic fractions of HMDMs and BMDMs (*Figure 1E*). To validate the NFATc3 down-regulation, we determined the NFATc3 mRNA levels in circulating PBMCs from patients with carotid atherosclerosis. NFATc3 mRNA levels were consistently lower in both asymptomatic and symptomatic patients than in the healthy controls. Notably, NFATc3 levels in symptomatic patients were lower than those in the asymptomatic patients (*Figure 1F*), suggesting that the decreased NFATc3 levels in macrophages may be causally related to plaque instability. Moreover, we explored the potential mechanism whereby oxLDL attenuates NFATc3 levels. c-Jun N-terminal kinase (JNK) signalling has been revealed to promote NFATc3 translocation from the nucleus to the cytoplasm.[18,19] Previous studies showed that JNK could be activated by oxLDL in macrophages.[17,20,21] We found that specific inhibition of JNK signalling led to the nuclear retention of NFATc3 (*Figure 1G*), indicating that JNK signalling activation contributes to the NFATc3 nuclear export during lipid challenge.

Deletion of NFATc3 in macrophages promotes atherogenesis in mice

To investigate the role of macrophage NFATc3 in atherosclerosis, we generated myeloid-specific NFATc3 knockout mice (*LysM*-Cre-*NFATc3*^{Flox}), hereafter referred to as *NFATc3*^{MKO} mice (Supplementary material online, *Figure S2A and B*). The null allele was confirmed in BMDMs from *NFATc3*^{MKO} mice. NFATc3 depletion did not alter the expression of other NFAT isoforms in macrophages (Supplementary material online, *Figure S2C*). Atherosclerosis was induced in mice via the tail-vein injection of an adeno-associated virus (AAV8) encoding the Asp374-to-Tyr mutant version of human *PCSK9* (*PCSK9*^{DY}) followed by HFD feeding (Supplementary material online, *Figure S2D*). The *PCSK9*^{DY} mutation directly targets hepatocytes by inducing degradation of hepatic low-density lipoprotein receptor (LDLR), therefore resembling that of *LDLR*$^{-/-}$ mice.[22] As expected, the LDLR protein was almost undetectable in the liver after AAV-*PCSK9*^{DY} infection (Supplementary material online, *Figure S2E*). Deletion of NFATc3 in macrophages did not affect the body weight or serum lipid levels of mice fed a chow diet or HFD (Supplementary material online, *Figure S2F–J*). No distinct plaques were observed in chow diet-fed *NFATc3*^{Flox} or *NFATc3*^{MKO} mice after AAV-*PCSK9*^{DY} infection. Notably, *NFATc3*^{MKO} mice fed an HFD showed larger plaque areas in aortas and aortic roots than HFD-fed *NFATc3*^{Flox} mice, as assessed by Oil Red O staining (*Figure 2A and B*). Further analysis of the plaques in aortic roots revealed that the atherosclerotic lesion and necrotic core areas were increased, but the collagen content decreased in *NFATc3*^{MKO} mice (*Figure 2C–E*). More detailed assessment of the composition of aortic root plaques indicated that *NFATc3*^{MKO} mice

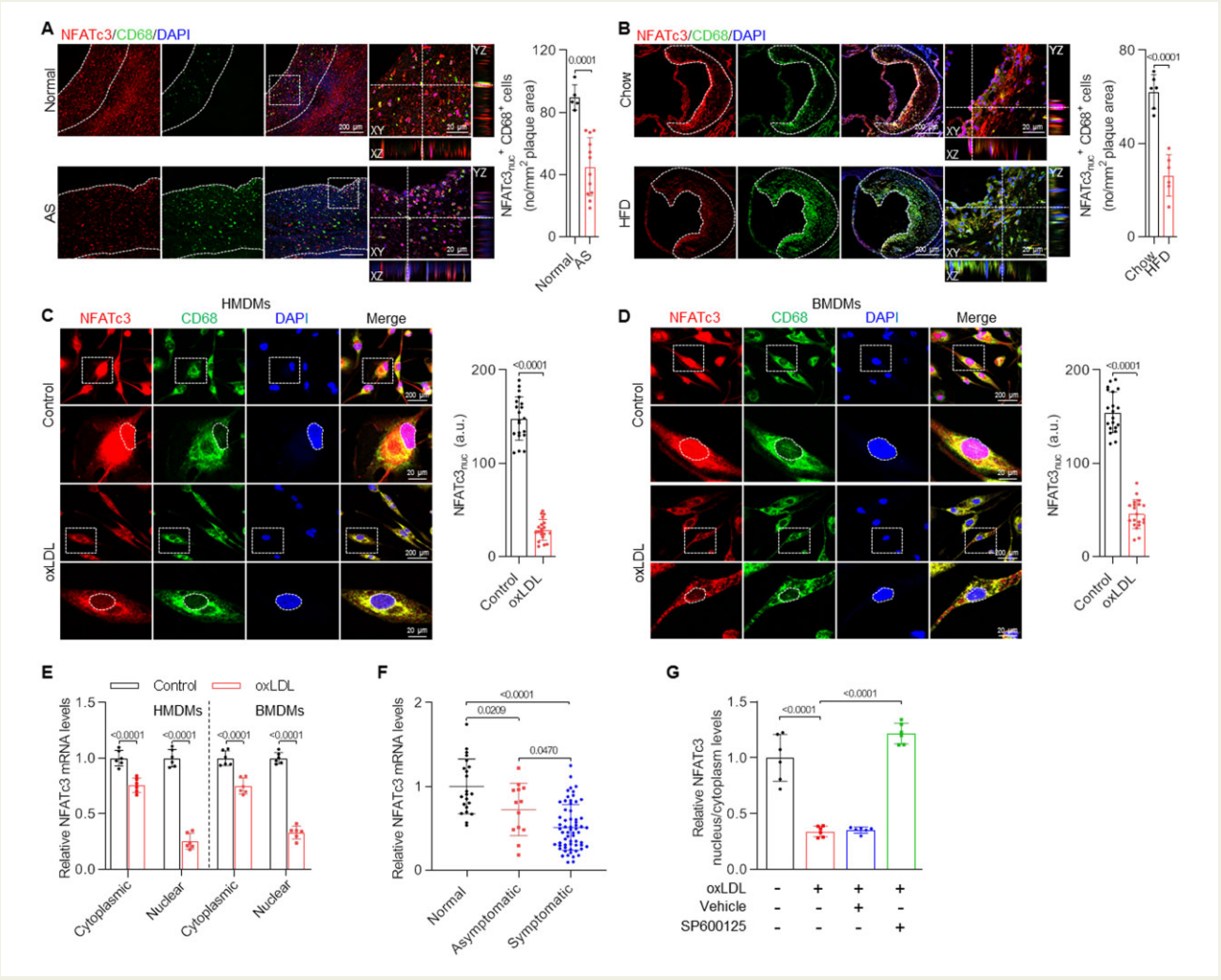

Figure 1 Reduced NFATc3 expression in the peripheral blood mononuclear cells of atherosclerosis patients is correlated with symptoms of instability. Representative immunofluorescence images for NFATc3 and CD68 in the plaques of normal arteries derived from healthy control individuals ($n = 5$) and of carotid arteries derived from carotid atherosclerosis patients ($n = 12$) (*A*) and in the plaques of the aortic sinuses from *Apoe*$^{-/-}$ mice fed with the chow diet ($n = 6$) or high-fat diet ($n = 6$) for 12 weeks (*B*). Quantification of the numbers of cells expressing NFATc3 in nucleus ($NFATc3_{nuc}$) and CD68 within the plaque lesions. Immunofluorescence detection of NFATc3 and CD68 in human monocyte-derived macrophages (*C*) and mouse bone marrow-derived macrophages (*D*) cultured with oxidized low-density lipoproteins (80 μg/mL) for 24 h. The fluorescence intensity of NFATc3 in the nucleus was quantified. $n = 20$ cells. (*E*) qRT-PCR analysis of the NFATc3 mRNA levels in the cytoplasm and nucleus ($n = 6$). (*F*) The NFATc3 mRNA levels in the peripheral blood mononuclear cells of healthy individuals (normal) ($n = 22$) and in the peripheral blood mononuclear cells of symptomatic ($n = 62$) and asymptomatic ($n = 13$) carotid atherosclerosis patients. (*G*) The relative levels of the nuclear vs. cytoplasmic NFATc3 mRNA levels in human monocyte-derived macrophages pretreated with the c-Jun N-terminal kinase inhibitor SP600125 (20 μmol/L) for 3 h before a 24-h oxidized low-density lipoproteins treatment ($n = 6$). Data are presented as the mean ± SD. (*A*–*E*) Unpaired Student's *t*-test was used; the two-tailed *P*-values are shown. (*F* and *G*) One-way ANOVA followed by Tukey's correction was used; the adjusted *P*-values are shown. AS, atherosclerosis; HFD, high-fat diet; oxLDL, oxidized low-density lipoproteins; a.u., arbitrary units; BMDM, bone marrow-derived macrophage; HMDM, human monocyte-derived macrophage.

showed a higher infiltration of $CD68^+$ macrophages and $CD3^+$ T cells (*Figure 2F and G*). However, the smooth muscle cell, dead cell, or proliferating cell content of the plaques was not altered (*Figure 2H* and Supplementary material online, *Figure S2K and L*).

Next, we performed bone marrow transplantation to confirm the effects of NFATc3 macrophage-specific ablation on atherosclerosis in an *Apoe*$^{-/-}$ background. *Apoe*$^{-/-}$ male mice were lethally irradiated and reconstituted with bone marrow from either *NFATc3*^{Flox} (*NFATc3*^{Flox}/*Apoe*$^{-/-}$) or *NFATc3*^{MKO} (*NFATc3*^{MKO}/*Apoe*$^{-/-}$) mice (*Figure 3A*). Successful bone marrow chimaera generation was verified by PCR of genomic DNA from peripheral blood (*Figure 3B*). The atherosclerotic plaque areas in aortas and aortic roots were increased in *Apoe*$^{-/-}$ mice that received the bone marrow from *NFATc3*^{MKO} mice (*Figure 3C and D*). The aortic roots from *NFATc3*^{MKO}/*Apoe*$^{-/-}$ chimaeras exhibited larger lesions and necrotic core areas than those from *NFATc3*^{Flox}/*Apoe*$^{-/-}$ chimaeras (*Figure 3E and F*). In addition, the

collagen content was decreased in the plaques of *NFATc3*^{MKO}/*Apoe*$^{-/-}$ chimaeras, while the macrophage and T-cell counts increased (*Figure 3G–I*). No significant differences in body weight or serum lipid levels were found between the two groups (Supplementary material online, *Figure S3*).

NFATc3 overexpression inhibits atherosclerosis and inflammation

To further verify the functional role of macrophage NFATc3 in atherosclerosis, we established macrophage-specific NFATc3 transgenic mice (*NFATc3*^{MTG}), which were crossed with *Apoe*$^{-/-}$ mice to obtain *NFATc3*^{MTG}/*Apoe*$^{-/-}$ mice (Supplementary material online, *Figure S4A–C*). NFATc3 expression was higher in thioglycollate-elicited peritoneal macrophages (TEPMs) from *NFATc3*^{MTG}/*Apoe*$^{-/-}$ mice than in those from *Apoe*$^{-/-}$ mice (Supplementary material online, *Figure S4D*). The body weight and serum lipid levels of *NFATc3*^{MTG}/*Apoe*$^{-/-}$ mice were not different from those of *Apoe*$^{-/-}$ mice fed a chow diet or HFD (Supplementary material online, *Figure S4E–I*). The total plaque areas were comparable between the mice with either genotype that received a chow diet. However, after HFD feeding, the plaque areas in *NFATc3*^{MTG}/*Apoe*$^{-/-}$ mice decreased relative to those in *Apoe*$^{-/-}$ mice (*Figure 4A and B*). In addition, reduced lesion and necrotic core areas and increased collagen content were observed in the aortic roots of *NFATc3*^{MTG}/*Apoe*$^{-/-}$ mice (*Figure 4C–E*). The infiltration of macrophages and T cells in plaques was inhibited in these mice, compared with that in *Apoe*$^{-/-}$ mice (*Figure 4F and G*). However, the number of dead or proliferating cells did not change (Supplementary material online, *Figure S4J and K*). Serum levels of monocyte chemotactic protein (MCP)-1 and interleukin (IL)-1β decreased significantly, whereas the IL-6 and IL-10 levels increased in *NFATc3*^{MTG}/*Apoe*$^{-/-}$ mice (*Figure 4H*). In vehicle- (resting), lipopolysaccharide/interferon-γ (LPS/IFN-γ)-, or IL-4-treated TEPMs, NFATc3 overexpression was associated with increased IL-10 mRNA levels. In addition, *NFATc3*^{MTG} TEPMs showed decreased MCP-1 mRNA levels and increased arginase 1 mRNA levels upon LPS/IFN-γ or IL-4 treatment. Of note, in contrast to resting or IL-4-treated macrophages, NFATc3 up-regulation decreased IL-6 mRNA levels in LPS/IFN-γ-treated TEPMs (*Figure 4I*). Together, these results suggest that NFATc3 converts pro-inflammatory macrophages into those with an anti-inflammatory phenotype.

NFATc3 depletion promotes foam cell formation and scavenger receptor expression

Next, we examined the potential role of NFATc3 in the formation of macrophage-derived foam cells. *NFATc3*^{MKO} BMDMs showed enhanced foam cell formation and lipid accumulation compared with *NFATc3*^{Flox} BMDMs (*Figure 5A–C*). The opposite effects were observed in NFATc3-overexpressing TEPMs (Supplementary material online, *Figure S5A–C*). To investigate whether the increased binding or uptake of modified lipoproteins accounts for the enhanced foam cell formation in NFATc3-deficient macrophages, we performed the binding and uptake assay with Dil-oxLDL. Immunofluorescence revealed that the oxLDL-induced increase in Dil-oxLDL binding and uptake was potentiated in *NFATc3*^{MKO} BMDMs but suppressed in *NFATc3*^{MTG} TEPMs (*Figure 5D and E* and Supplementary material online, *Figure S5D and E*). To delineate the mechanism whereby NFATc3 ablation increases foam cell formation, the expression of scavenger receptors and transporters was determined. Deletion of NFATc3 increased SR-A and CD36 expression in BMDMs and TEPMs, but barely affected the expression of scavenger receptor LOX-1 or cholesterol transporters, such as SRB-1 and ABCG1 (*Figure 5F* and Supplementary material online, *Figure S6A*). Interestingly, knockdown of NFATc1, NFATc2, or NFATc4 in TEPMs did not alter the expression of SR-A or CD36 (Supplementary material online, *Figure S6B*). Immunofluorescence measurement confirmed that the SR-A and CD36 levels were increased in macrophages within the lesions of *NFATc3*^{MKO} mice compared with those in *NFATc3*^{Flox} mice (*Figure 5G*). Conversely, the TEPMs and aortic roots from *NFATc3*^{MTG} mice showed a decreased SR-A and CD36 expression (Supplementary material online, *Figure S6C–E*). The enhanced foam cell formation, as well as oxLDL binding and uptake, was suppressed upon the antibody-mediated neutralization of SR-A or CD36. Importantly, the neutralization of both SR-A and CD36 exhibited clear synergistic effects (Supplementary material online, *Figure S7*). These findings indicate that the proatherogenesis in *NFATc3*^{MKO} mice results from the up-regulation of SR-A and CD36 in macrophages.

Correlation analysis revealed that the PBMC NFATc3 levels were negatively correlated with the SR-A and CD36 levels in normal controls and carotid atherosclerosis patients (*Figure 5H and I*), further suggesting that NFATc3 regulates SR-A and CD36 expression. We searched for potential NFATc3-binding sites in the promoters of SR-A and CD36 (within the -2.0 kb fragment upstream of the transcription start site) by using the JASPAR database. Consequently, four potential sites were predicted in each promoter region. However, ChIP-qPCR revealed that the NFATc3 enrichment on either sites of the SR-A and CD36 promoter fragments did not differ from IgG control (Supplementary material online, *Figure S8A*). We also assessed whether NFATc3 directly binds to SR-A and CD36 at the mRNA or protein levels but observed no such interaction (Supplementary material online, *Figure S8B–E*). Collectively, these results suggest that NFATc3 is unlikely to suppress SR-A and CD36 transcription by directly targeting their promoters.

MiR-204 is a direct target of NFATc3

Given that microRNAs (miRNAs) are found to inhibit the expression of most regulated genes, we assessed whether miRNAs relay NFATc3 to the inhibition of SR-A and CD36 expression. To identify the candidate miRNAs, small RNA sequencing was performed on *NFATc3*^{MTG} TEPMs in comparison with wild-type TEPMs. Of the annotated miRNAs, 26 were significantly dysregulated in *NFATc3*^{MTG} TEPMs compared with wild-type TEPMs (Supplementary material online, *Figure S9A*). The top 5 up-regulated miRNAs were further validated using qRT-PCR (*Figure 6A*). We also performed a small RNA microarray on Ad-NFATc3-treated HMDMs in comparison with the control group (*Figure 6B* and Supplementary material online, *Figure S9B*). The intersection of both miRNA profiling results revealed that only miRNA-204-3p was up-regulated after NFATc3 overexpression. Although miR-204-5p increased only in *NFATc3*^{MTG} TEPMs, the microarray analysis of HMDMs lacked the probe targeting miR-204-5p. Therefore, we additionally examined the levels of miR-204-5p in HMDMs by qRT-PCR. Consistent with the data from TEPMs, miR-

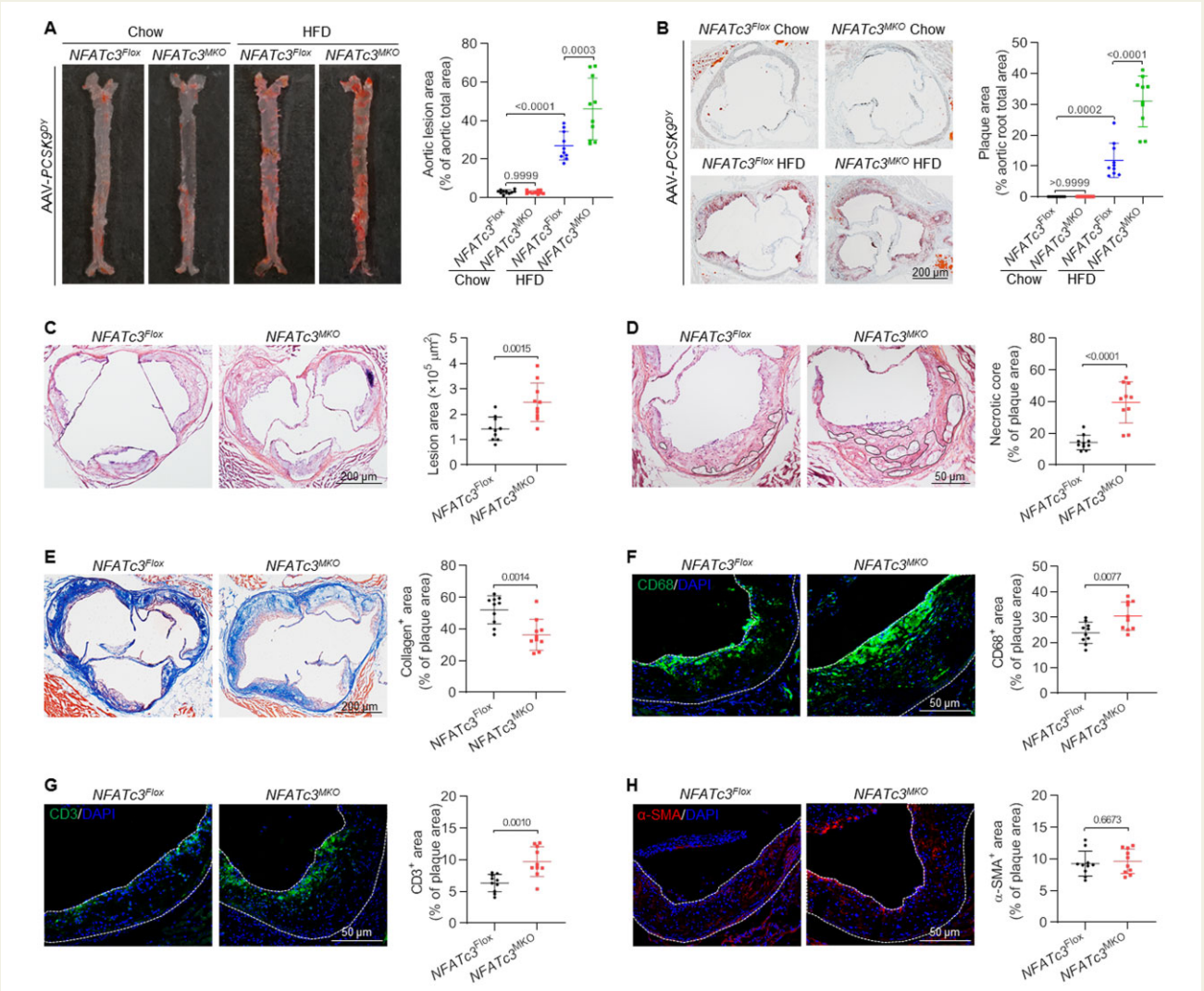

Figure 2 NFATc3 deficiency exacerbates AAV-*PCSK9*^{DY}-induced atherosclerosis. (*A*) Representative images of the *en face* Oil Red O-stained aortas from the *NFATc3*^{Flox} or *NFATc3*^{MKO} mice that were administered AAV-*PCSK9*^{DY} followed by 12 weeks of chow diet or high-fat diet feeding. Quantification of the mean aortic lesion area in each group as a percentage of the mean aortic area. (*B*) Representative microphotographs and quantification of the Oil Red O-stained aortic root sections from the mice of each genotype. Lesion formation (*C*) and necrotic core area (*D*) in the aortic roots after a 12-week high-fat diet regimen. (*E*) Representative images and collagen quantification of the aortic roots stained with Masson's trichrome stain. Representative image of plaque within the aortic root subjected to immunofluorescent staining for the macrophage marker CD68 (*F*), T-lymphocyte marker CD3 (*G*), or smooth muscle cell marker α-SMA (*H*), and the corresponding quantification results. Data are presented as the mean ± SD ($n = 10$ per group). (*A* and *B*) Two-way ANOVA with Tukey's correction was used; the adjusted *P*-values are shown. For (*C*)–(*H*), unpaired Student's *t*-test was used; the two-tailed *P*-values are shown. AAV, adeno-associated virus; HFD, high-fat diet.

204-5p was also up-regulated in Ad-NFATc3-treated HMDMs (*Figure 6B*). The luciferase assay showed that NFATc3 up-regulation led to a 4-fold increase in miR-204 promoter activity, and a serial promoter deletion analysis further showed that the functional NFATc3 site was centred on an evolutionarily conserved site that is approximately -1.5 kb upstream of the miR-204 gene (*Figure 6C* and Supplementary material online, *Figure S9C*). ChIP-qPCR results confirmed that NFATc3 was enriched in this region of the miR-204 promoter (*Figure 6D*), suggesting that NFATc3 directly targets miR-204. miR-204 is an evolutionarily conserved miRNA located in intron 6 of the human TRPM3 gene, and the NFATc3-binding site on the miR-204 promoter is located in intron 1 of the TRPM3 gene (Supplementary material online, *Figure S9D*). NFATc3 up-regulation increased the levels of miR-204 precursor (*pre-miR-204*) in TEPMs and HMDMs but did not alter TRPM3 expression (Supplementary material online, *Figure S9E and F*), indicating that NFATc3 up-regulates miR-204 independent of the host gene.

To determine whether the NFATc3-mediated regulation of miR-204 is implicated in atherosclerosis, the *pre-miR-204* levels in PBMCs and plaques of atherosclerotic patients were examined. The *pre-miRNA-204* levels were decreased in PBMCs and plaques from atherosclerosis patients, and a positive correlation

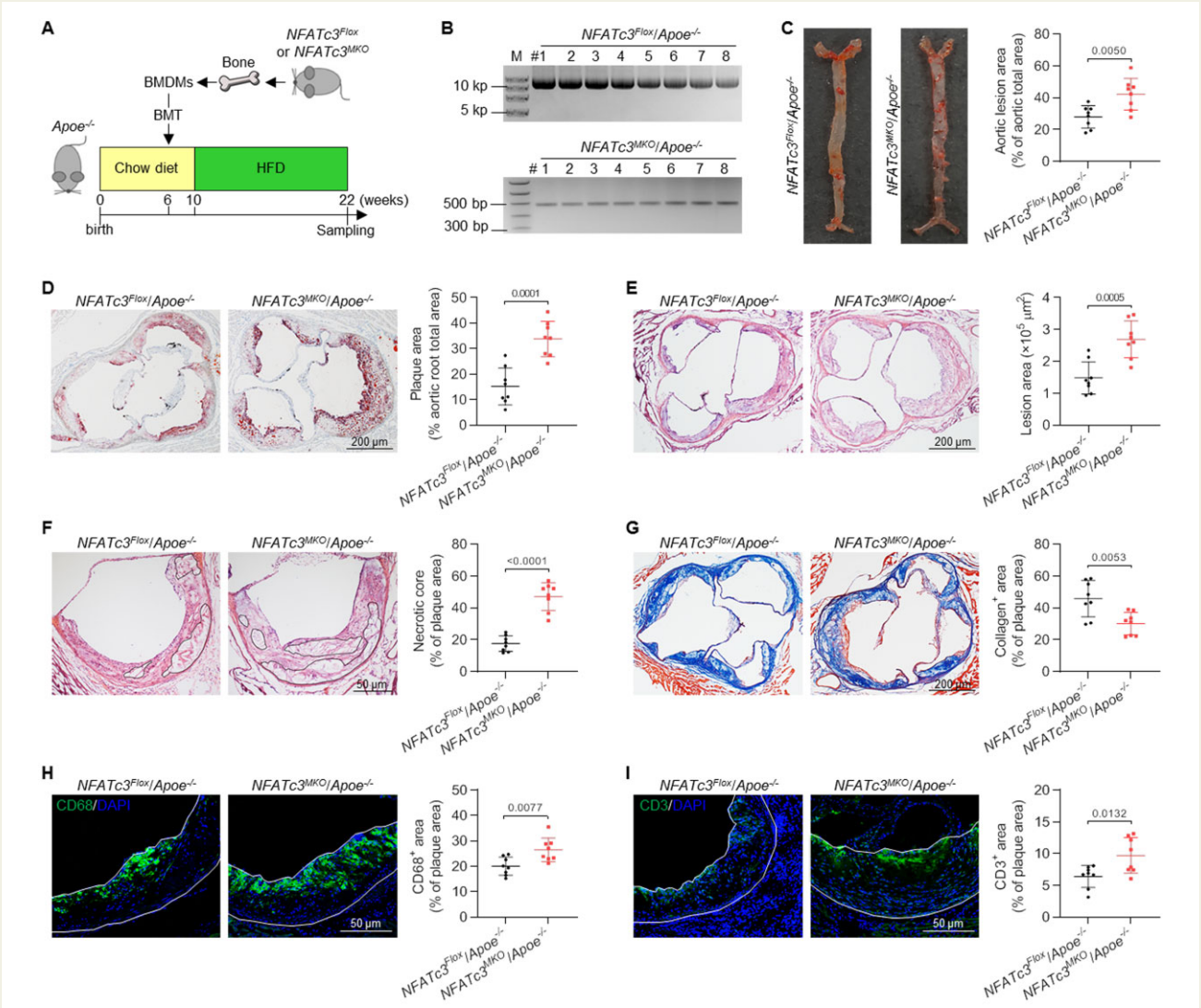

Figure 3 The absence of NFATc3 in bone marrow-derived cells promotes atherosclerotic lesion formation in chimaeric *Apoe*$^{-/-}$ mice. (*A*) Flowchart illustrating the experimental procedure of bone marrow transplantation in *Apoe*$^{-/-}$ mice. (*B*) PCR analysis for NFATc3 alleles in the peripheral blood from irradiated *Apoe*$^{-/-}$ mice transplanted with *NFATc3*^{Flox} or *NFATc3*^{MKO} bone marrow. The PCR products for the *NFATc3*^{Flox} and *NFATc3*^{MKO} alleles are 11 665 and 487 bp in length, respectively. (*C*) Representative images of Oil Red O-stained aortas from chimaeric *Apoe*$^{-/-}$ mice that received bone marrow cells from *NFATc3*^{Flox} or *NFATc3*^{MKO} mice after a 12-week high-fat diet. The mean plaque area in the aortas was quantitated based on the Oil Red O staining results. Representative microphotographs of the plaque area (*D*), lesion formation (*E*), necrotic core area (*F*), and collagen content (*G*) in the aortic roots of the chimaeric *Apoe*$^{-/-}$ mice, and the corresponding quantification results. Representative microphotographs showing macrophage (*H*) and T-lymphocyte (*I*) accumulation in the atherosclerotic plaques of chimaeric *Apoe*$^{-/-}$ mice, and the corresponding quantification results. Data are presented as the mean ± SD and analysed using unpaired Student's *t*-test; the two-tailed *P*-values are shown ($n = 8$ per group). BMDM, bone marrow-derived macrophage; BMT, bone marrow transplantation.

between NFATc3 and *pre-miR-204* levels was found in PBMCs (*Figure 6E–G*). Similar findings were obtained in the aortic roots of HFD-fed *Apoe*$^{-/-}$ mice vs. chow diet-fed *Apoe*$^{-/-}$ mice (*Figure 6G*). In addition, oxLDL stimulation decreased the enrichment of NFATc3 on the miR-204 promoter (*Figure 6H*). Concomitantly, oxLDL also inhibited the transcription of miR-204; this effect was antagonized by NFATc3 up-regulation (*Figure 6I*). These findings suggest that the inhibition of NFATc3 nuclear accumulation upon an atherogenic challenge contributes to the decreased binding of NFATc3 to the miR-204 promoter, leading to miR-204 transcriptional repression.

To clarify the relevant role of miR-204 in NFATc3-mediated scavenger receptor expression and foam cell formation, we treated macrophages with either mature miR-204-5p or miR-204-3p mimics. The SR-A expression was decreased in BMDMs, TEPMs, HMDMs, and Raw 264.7 cells treated with miR-204-5p mimics, whereas the CD36 expression was not altered (*Figure 6J*). Interestingly, miR-204-3p decreased CD36 expression but barely

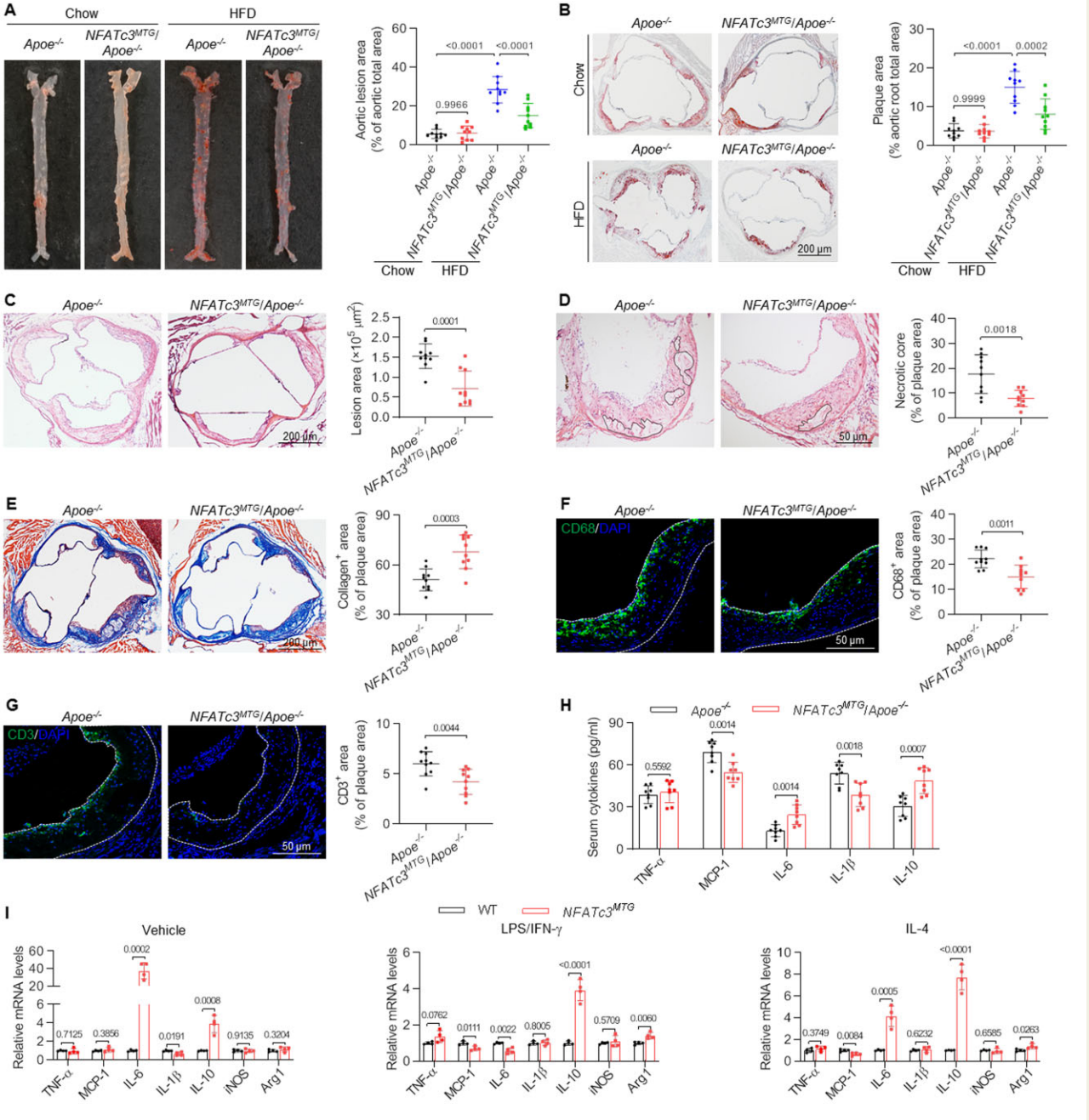

Figure 4 NFATc3 up-regulation suppresses atherosclerosis in *Apoe*$^{-/-}$ mice. Representative images of the Oil Red O-stained aortas (*A*) and aortic roots (*B*) of *Apoe*$^{-/-}$ and *NFATc3*^{MTG}/*Apoe*$^{-/-}$ mice fed with the chow diet or high-fat diet for 12 weeks ($n = 10$ per group). (*C*–*G*) Representative images of the aortic root sections isolated from the *Apoe*$^{-/-}$ or *NFATc3*^{MTG}/*Apoe*$^{-/-}$ mice fed the high-fat diet for 12 weeks. The sections were stained with haematoxylin and eosin (*C* and *D*), or Masson's trichrome stain (*E*), or immunostained for CD68 (*F*) or CD3 (*G*). The quantification results are shown on the right ($n = 10$ per group). (*H*) Serum levels of TNF-α, MCP-1, IL-6, IL-1β, and IL-10 in *Apoe*$^{-/-}$ or *NFATc3*^{MTG}/*Apoe*$^{-/-}$ mice after a 12-week high-fat diet ($n = 8$ per group). (*I*) The mRNA levels of cytokines or genes in wild-type or *NFATc3*^{MTG} thioglycollate-elicited peritoneal macrophages treated as indicated ($n = 4$). Data are presented as the mean ± SD. (*A* and *B*) Two-way ANOVA with Tukey's correction was used; the adjusted *P*-values are shown. For (*C*)–(*I*), unpaired Student's *t*-test was used; the two-tailed *P*-values are shown. HFD, high-fat diet; WT, wild-type; LPS/IFN-γ, lipopolysaccharide/interferon-γ; TNF-α, tumor necrosis factor-α; MCP-1, monocyte chemotactic protein-1; IL, interleukin; iNOS, inducible nitric oxide synthase; Arg1, arginase 1.

affected SR-A expression in macrophages (*Figure 6K*). In BMDMs from *NFATc3*^{MKO} mice, miR-204-5p inhibited SR-A up-regulation, while miR-204-3p was associated with decreased CD36 expression (*Figure 6L*). Importantly, deletion of the NFATc3-binding site on the miR-204 promoter using the CRISPR/Cas9 system abrogated the effects of NFATc3 on SR-A and CD36

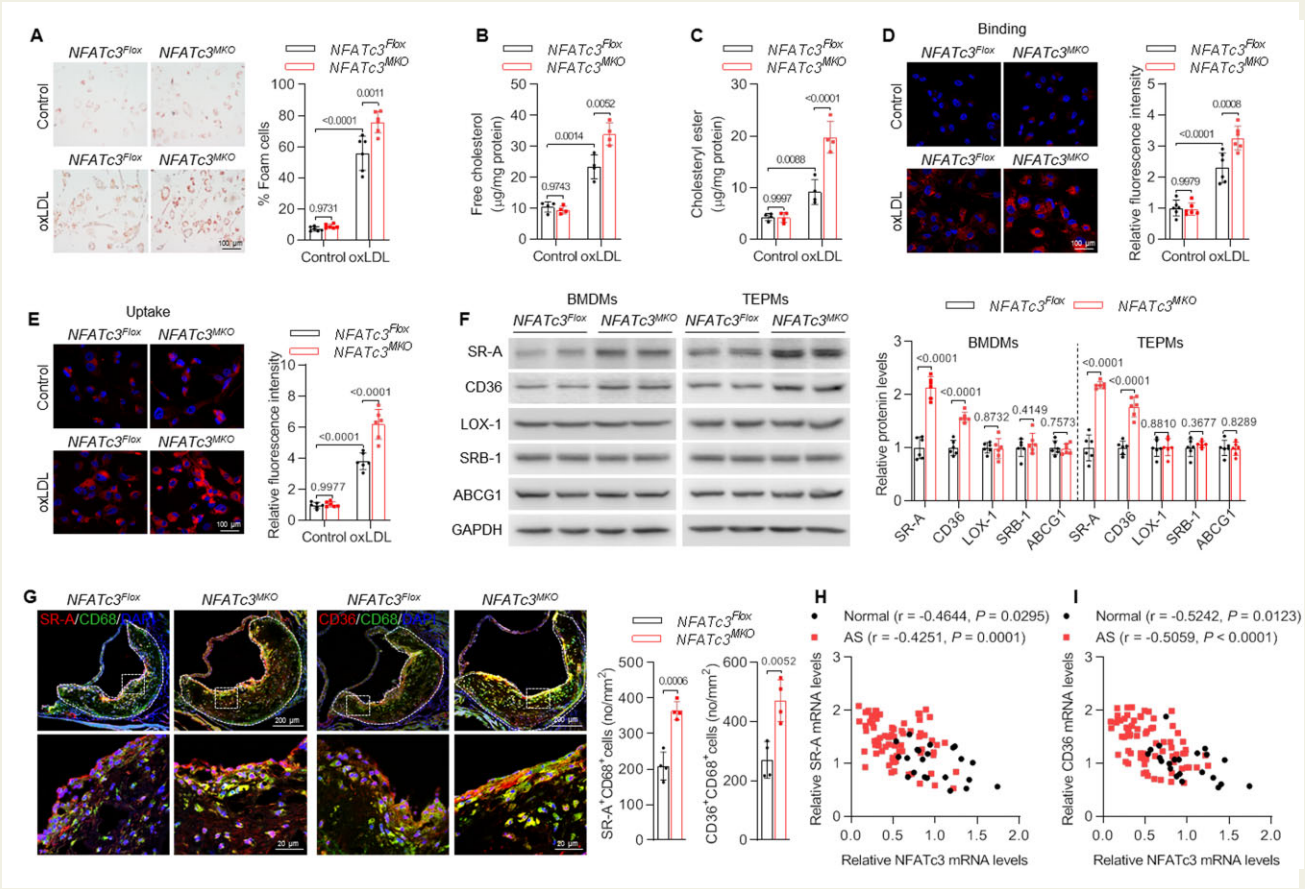

Figure 5 NFATc3 ablation enhances foam cell formation and scavenger receptor expression. (*A*) Representative microphotographs and quantification of foam cells in *NFATc3*^{Flox} or *NFATc3*^{MKO} bone marrow-derived macrophages cultured with or without oxidized low-density lipoproteins for 24 h ($n = 6$). Accumulation of unesterified cholesterol (*B*) and cholesteryl ester (*C*) in *NFATc3*^{Flox} or *NFATc3*^{MKO} bone marrow-derived macrophages treated with or without oxidized low-density lipoproteins for 24 h ($n = 4$). Representative images showing the binding (*D*) and uptake (*E*) of DiI-labelled oxidized low-density lipoproteins. The quantification results are shown on the right ($n = 6$). (*F*) SR-A, CD36, LOX-1, SRB-1, and ABCG1 protein levels in bone marrow-derived macrophages and thioglycollate-elicited peritoneal macrophages isolated from *NFATc3*^{Flox} or *NFATc3*^{MKO} mice ($n = 6$ per group). (*G*) Double-immunofluorescence staining for CD68 and SR-A, or CD68 and CD36 in the aortic roots from *NFATc3*^{Flox} or *NFATc3*^{MKO} mice after a 12-week high-fat diet. Quantification of SR-A^{+}CD68^{+} or CD36^{+}CD68^{+} cell numbers in the plaque lesions ($n = 4$ per group). (*H* and *I*) *NFATc3* mRNA levels negatively correlate with SR-A (*H*) or CD36 (*I*) levels in the peripheral blood mononuclear cells of healthy control individuals and peripheral blood mononuclear cells of patients with carotid atherosclerotic diseases (including asymptomatic and symptomatic patients). Data are presented as the mean ± SD. (*A*–*E*) Two-way ANOVA with Tukey's correction was used; the adjusted *P*-values are shown. (*F* and *G*) Unpaired Student's *t*-test was used; the two-tailed *P*-values are shown. (*H* and *I*) Pearson correlation coefficient test was used; the regression coefficients and two-tailed *P*-values are shown. oxLDL, oxidized low-density lipoproteins; AS, atherosclerosis; BMDM, bone marrow-derived macrophage; TEPM, thioglycollate-elicited peritoneal macrophage.

expression (Supplementary material online, *Figure S9G and H*), thus confirming the role of miR-204 in NFATc3-mediated inhibition of scavenger receptor expression. miR-204-5p or miR-204-3p up-regulation offset the enhanced effects of NFATc3 deficiency on foam cell formation and lipid accumulation, whereas the inhibitory effects observed in *NFATc3*^{MTG} TEPMs were reversed by miR-204-5p or miR-204-3p inhibitor. The combination of the mimics or inhibitors showed stronger effects than the individual treatments (Supplementary material online, *Figures S10 and S11*). In addition, the *pre-miR-204* levels were lower and SR-A and CD36 expression were higher in LPS/IFN-γ-treated HMDMs than in IL-4-treated cells (*Figure 6M*), suggesting that the alterations in miR-204/scavenger receptors axis during inflammatory state transitions are associated with the atheroprotection of macrophage NFATc3.

Furthermore, bioinformatics analysis revealed an evolutionarily conserved miR-204-5p seed region within the 3′-untranslated region (3′-UTR) of SR-A (Supplementary material online, *Figure S12A*). Transfection of miR-204-5p mimics decreased the SR-A 3′-UTR reporter activity; this effect was not observed when the seed region was mutated (Supplementary material online, *Figure S12B*). Although an miR-204-3p seed region was found in human and rat CD36 3′-UTRs, miR-204-3p did not alter the activity of CD36 3′-UTR reporter (Supplementary material online, *Figure S12C and D*). Transfection

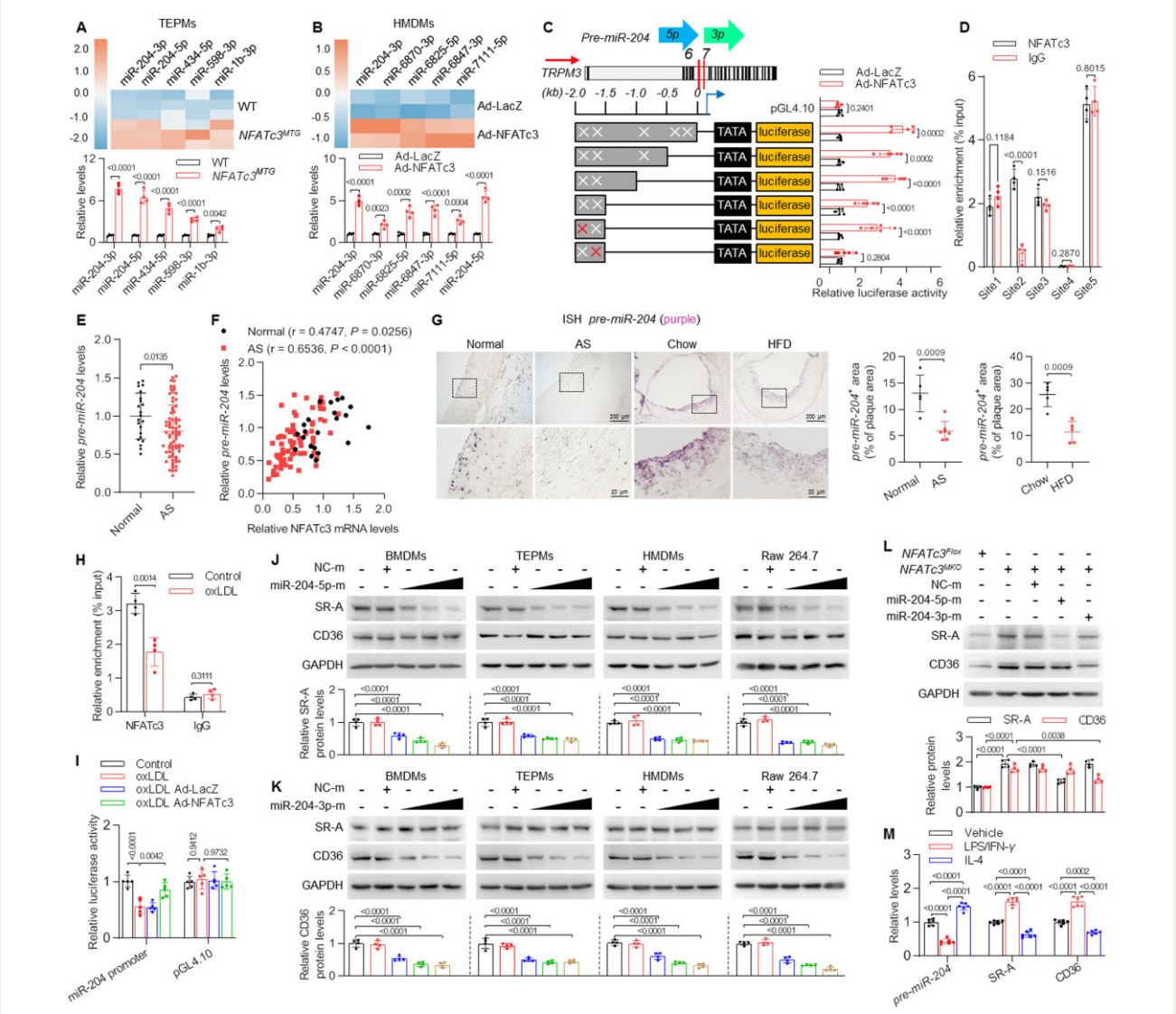

Figure 6 NFATc3 targets miR-204. (*A*) Heat map of miRNA sequencing of *NFATc3*^{MTG} thioglycollate-elicited peritoneal macrophages in comparison with wild-type thioglycollate-elicited peritoneal macrophages (upper panel, $n = 3$ per group). The selected miRNAs were confirmed by qRT-PCR (lower panel, $n = 4$ per group). (*B*) Heat map of the up-regulated miRNAs in the Ad-NFATc3-administered human monocyte-derived macrophages, as determined via microarray analysis (upper panel, $n = 2$), and qRT-PCR confirmation of the up-regulated miRNAs in human monocyte-derived macrophages (lower panel, $n = 4$). (*C*) MiR-204 promoter activity in HEK293T cells in response to Ad-NFATc3 infection. The analysis included site-directed mutations or serial deletions of the promoter ($n = 5$). (*D*) ChIP-qPCR analysis of NFATc3 enrichment on the miR-204 promoter in human monocyte-derived macrophages ($n = 4$). (*E*) The levels of miRNA-204 precursor (*pre-miR-204*) in peripheral blood mononuclear cells from the subjects without atherosclerosis ($n = 22$) vs. those in patients with carotid atherosclerosis (including asymptomatic and symptomatic patients; $n = 75$). (*F*) Correlative analysis of NFATc3 mRNA levels and *pre-miR-204* levels. (*G*) *In situ* hybridization of *pre-miR-204* in the plaques of normal arteries ($n = 5$) derived from healthy controls, the plaques of carotid arteries derived from carotid atherosclerotic patients ($n = 7$), and the plaques of aortic roots from the chow diet-fed ($n = 5$) or high-fat diet-fed ($n = 5$) *Apoe*$^{-/-}$ mice. (*H*) ChIP-qPCR analysis of the recruitment of NFATc3 to the miR-204 promoter upon oxidized low-density lipoproteins treatment in human monocyte-derived macrophages ($n = 4$). (*I*) Luciferase expression of the miR-204 promoter in human monocyte-derived macrophages infected with Ad-LacZ or Ad-NFATc3 for 24 h before a 24-h oxidized low-density lipoproteins treatment ($n = 5$). Expression levels of SR-A and CD36 in bone marrow-derived macrophages, thioglycollate-elicited peritoneal macrophages, human monocyte-derived macrophages, and Raw 264.7 cells treated with increasing concentrations of miR-204-5p mimics (miR-204-5p-m) (*J*) or miR-204-3p mimics (miR-204-3p-m) (*K*); NC-m, mimics negative control ($n = 4$). (*L*) Determination of SR-A and CD36 expression levels in the *NFATc3*^{MKO} bone marrow-derived macrophages transfected with the indicated constructs ($n = 4$). (*M*) The levels of *pre-miR-204*, SR-A and CD36 in human monocyte-derived macrophages treated as indicated ($n = 6$). Data are presented as the mean ± SD. (*A–D*, *G*, and *H*) Unpaired Student's *t*-test was used; the two-tailed *P*-values are shown. (*E*) Normality test failed, and Mann–Whitney *U* test with exact method was used; the two-tailed *P*-values are shown. (*F*) Pearson correlation coefficient test was used; the regression coefficients and two-tailed *P*-values are shown. One-way ANOVA was used with Tukey's correction (*I*, *L*, and *M*) or Dunnett's correction (*J* and *K*); the adjusted *P*-values are shown. Ad-LacZ, adenovirus harbouring LacZ; Ad-NFATc3, adenovirus harbouring NFATc3; oxLDL, oxidized low-density lipoproteins; HFD, high-fat diet; AS, atherosclerosis; BMDM, bone marrow-derived macrophage; HMDM, human monocyte-derived macrophage; TEPM, thioglycollate-elicited peritoneal macrophage; LPS/IFN-γ, lipopolysaccharide/interferon-γ; IL-4, interleukin-4.

of miR-204-3p with a mutated seed sequence had effects similar to those of the miR-204-3p mimics transfection on CD36 expression in HMDMs (Supplementary material online, *Figure S12E and F*). The half-life of CD36 mRNA in HMDMs was also not altered by miR-204-3p (Supplementary material online, *Figure S12G*).

Collectively, these results identified miR-204 as a candidate target of NFATc3. Canonical inhibition of SR-A by miR-204-5p and non-canonical inhibition of CD36 by miR-204-3p lead to suppressed foam cell formation.

MiRNA-204-3p localizes in the nucleus and inhibits CD36 transcription

The novelty of the miR-204-3p non-seed region repressing CD36 expression prompted us to explore the biogenesis and function of miR-204-3p in macrophages. To this end, we performed RNA sequencing in miR-204-3p mimics-treated HMDMs, confirming decreased CD36 expression upon miR-204-3p up-regulation, compared with the control group (Supplementary material online, *Figure S12H*). Further Gene Ontology analysis showed that the down-regulated genes were enriched in nuclear function-related biology processes (Supplementary material online, *Figure S12I*). Surprisingly, fluorescent *in situ* hybridization revealed that miR-204-3p was localized in the nuclei of macrophages, but not vascular smooth muscle cells or endothelial cells (*Figure 7A* and Supplementary material online, *Figure S13A and B*). qRT-PCR analysis further confirmed the nuclear presence of miR-204-3p, which was suppressed by oxLDL. However, the miR-204-3p levels in the cytoplasmic fractions remained unchanged upon oxLDL challenge (*Figure 7B*). Importantly, we observed little nuclear localization of miR-204-5p in HMDMs, excluding the possibility of the nuclear trapping of unprocessed *pre-miRNA-204* (Supplementary material online, *Figure S13C*). Both cytoplasmic *pre-miR-204* and miR-204-5p levels were decreased by oxLDL (Supplementary material online, *Figure S13D*). Since increasing evidence suggests that Argonaute 2 (Ago2) is critical for the functions of miRNAs in the nucleus,[23,24] we investigated whether nuclear miR-204-3p, together with Ago2, plays an epigenetic role in regulating CD36 expression. Ago2 was enriched in the nuclei of macrophages, and miR-204-3p co-immunoprecipitated with Ago2 from the nuclear extracts (*Figure 7C* and Supplementary material online, *Figure S13E–G*). The nuclear accumulation of Ago2 was increased in BMDMs from HFD-fed *Apoe*$^{-/-}$ mice and in oxLDL-treated HMDMs (*Figure 7D* and Supplementary material online, *Figure S13H*). Knockdown of Ago2 inhibited the oxLDL-induced CD36 up-regulation (Supplementary material online, *Figure S13I and J*). Both the luciferase reporter and nuclear run-on experiments showed an miR-204-3p-dependent down-regulation of the CD36 transcript levels; this effect was antagonized by Ago2 overexpression (*Figure 7E and F*). Nuclear Ago2 up-regulation also abolished the miR-204-3p-induced down-regulation of CD36 in HMDMs, and Ago2 knockdown suppressed the miR-204-3p inhibitor-induced CD36 up-regulation (*Figure 7G* and Supplementary material online, *Figure S13K and L*). Reciprocally, the Ago2 enrichment on the CD36 promoter was decreased by miR-204-3p in HMDMs (*Figure 7H*). Using the RNAhybrid website (https://bibiserv.cebitec.uni-bielefeld.de/rna-hybrid/), we observed a potential miR-204-3p target region present 100-bp upstream of the CD36 transcription start site (*Figure 7I*). Interestingly, the non-seed region of the miR-204-3p target sequence on the CD36 promoter is conserved between humans and mice (Supplementary material online, *Figure S13M*). The mutation of this region eliminated the miR-204-3p-induced inhibition of the CD36 promoter activity (*Figure 7J*), confirming the non-canonical inhibition of CD36 by miR-204-3p. Furthermore, Ago2 overexpression potentiated the oxLDL-induced increase in reporter activity; this increase was abolished when the binding site of miR-204-3p on the CD36 promoter was mutated (Supplementary material online, *Figure S13N*), indicating that miR-204-3p competes with Ago2 for the same binding region on the CD36 promoter. ChIP sequencing data revealed that miR-204-3p up-regulation decreased the enrichment of H3K27ac (enhancer and promoter marker) and H3K4me3 (promoter-specific marker) on the proximal promoter of CD36 in HMDMs; this was quantified and validated by ChIP-qPCR (*Figure 7K and L*).

Collectively, our data establish that miR-204-3p binds to a complementary target site within the CD36 promoter, thereby displacing the binding of Ago2 to CD36, consequently suppressing CD36 transcription.

MiR-204 mediates the atheroprotective effects of NFATc3

To establish the functional connection between NFATc3 and miR-204 in an atherosclerosis model, an AAV harbouring the miR-204 precursor (AAV-*pre-miR-204*) or LacZ (AAV-LacZ) was constructed and injected into *NFATc3*^{MKO} mice after 4 weeks of HFD feeding; the injection process lasted for 8 weeks (*Figure 8A*). Higher levels of *pre-miR-204* were observed in TEPMs and aortic roots of the mice treated with AAV-*pre-miR-204* (Supplementary material online, *Figure S14A and B*). AAV-*pre-miR-204* administration had no marked effects on body weight gain or serum lipid levels in HFD-fed *NFATc3*^{MKO} mice (Supplementary material online, *Figure S14C–G*). In TEPMs isolated from AAV-*pre-miR-204*-treated *NFATc3*^{MKO} mice, the SR-A and CD36 levels decreased compared with those in TEPMs from AAV-LacZ-treated *NFATc3*^{MKO} mice (*Figure 8B*). AAV-*pre-miR-204* administration also inhibited plaque formation in the aortas and aortic roots, accompanied by decreases in the necrotic core areas and the numbers of infiltrated inflammatory cells, and an increase in the collagen content (*Figure 8C–I*). In addition, we constructed an AAV harbouring an miR-204-5p or miR-204-3p inhibitor based on a tough decoy system and then injected the virus into *NFATc3*^{MTG} mice, followed by HFD feeding (Supplementary material online, *Figure S15A*). Blockade of miR-204-5p or miR-204-3p almost completely reversed the NFATc3-induced SR-A and CD36 down-regulation and atherosclerotic plaque formation (Supplementary material online, *Figure S15B–I*). These findings suggest that miR-204 is required for the atheroprotective effects of NFATc3.

Discussion

The impact of NFATs on the development of atherosclerosis remains controversial. The present study demonstrates that the nuclear

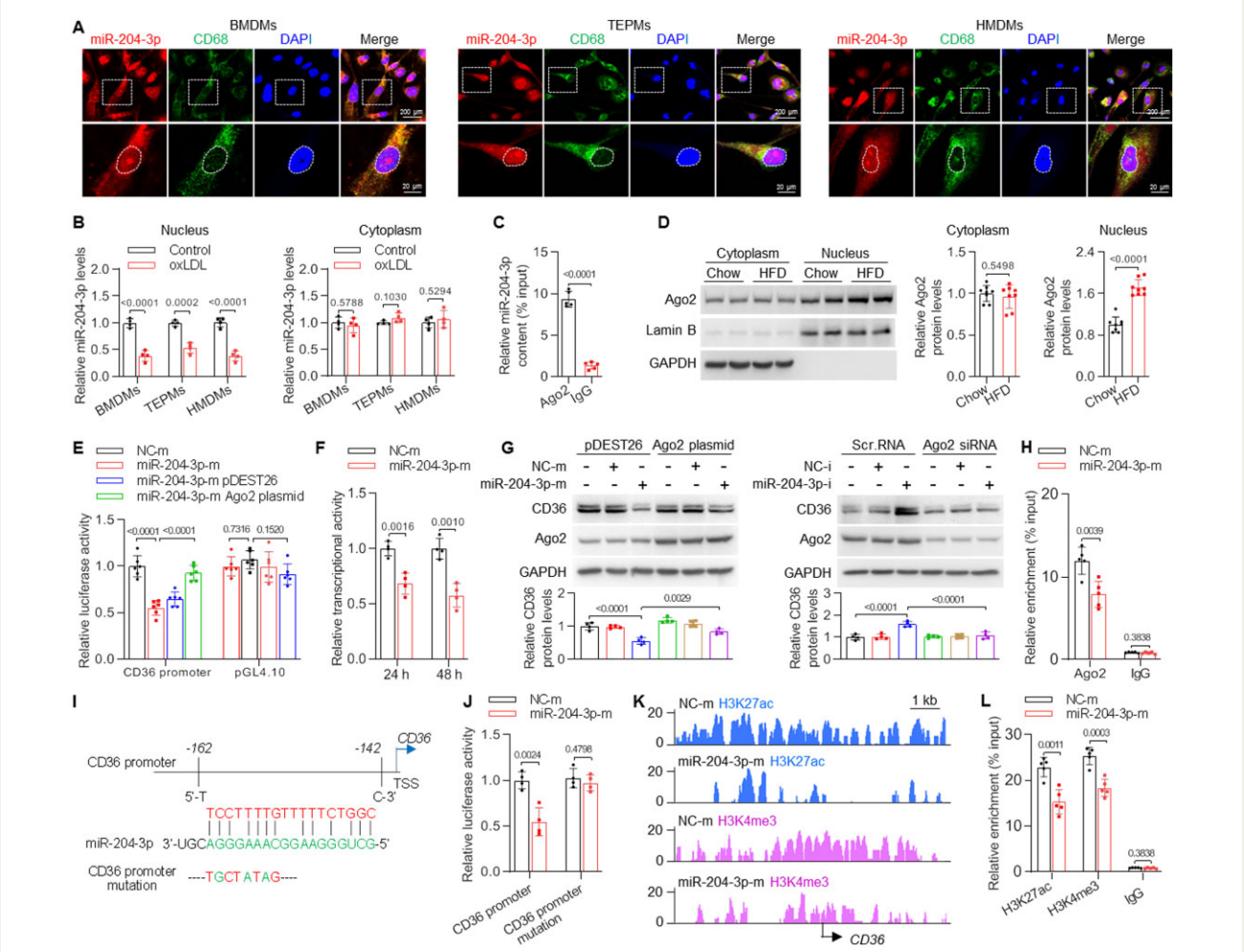

Figure 7 Nuclear miR-204-3p inhibits the transcription of CD36. (*A*) Immunofluorescence detection of miR-204-3p and CD68 in bone marrow-derived macrophages, thioglycollate-elicited peritoneal macrophages, and human monocyte-derived macrophages ($n = 5$). (*B*) qRT-PCR quantitation of the miR-204-3p levels in the nucleus and cytoplasm of bone marrow-derived macrophages, thioglycollate-elicited peritoneal macrophages, and human monocyte-derived macrophages treated with oxidized low-density lipoproteins for 24 h ($n = 4$). (*C*) RIP analysis of the nuclear fractions of human monocyte-derived macrophages by using anti-Ago2 or IgG antibody ($n = 5$). (*D*) The levels of Ago2 in the cytoplasm and nucleus of bone marrow-derived macrophages isolated from *Apoe*$^{-/-}$ mice fed with the chow diet or high-fat diet for 12 weeks ($n = 8$ per group). (*E*) Luciferase activity of the CD36 promoter in HEK293T cells transfected with the miR-204-3p mimics in the presence or absence of an Ago2 expression plasmid for 24 h. The pDEST26 plasmid was used as a negative control ($n = 6$). (*F*) Nuclear run-on assay for the assessment of the nascent CD36 mRNA level in human monocyte-derived macrophages for 24 or 48 h after transfection with the indicated constructs ($n = 4$). (*G*) The effects of miR-204-3p on CD36 expression were rescued by Ago2 up-regulation, whereas Ago2 knockdown abolished the effects of the miRNA-204-3p inhibitor on CD36 expression ($n = 4$). (*H*) ChIP-qPCR analysis of Ago2 recruitment on the CD36 promoter in human monocyte-derived macrophages IgG was used as a control antibody ($n = 5$). (*I*) Schematic illustration of the potential binding site of miR-204-3p on the human CD36 promoter. (*J*) Luciferase activity of the intact or mutated CD36 promoter in HEK293T cells transfected with the miR-204-3p mimics ($n = 4$). (*K*) UCSC genome-browser tracks of the H3K27ac and H3K4me3 peak distribution at the proximal promoter of CD36 in human monocyte-derived macrophages transfected with the indicated constructs for 24 h. (*L*) ChIP-qPCR validation of H3K27ac and H3K4me3 enrichment on the CD36 promoter ($n = 5$). Data are presented as the mean ± SD. (*B–D, F, H, J*, and *L*) Unpaired Student's *t*-test was used; the two-tailed *P*-values are shown. (*E*) One-way ANOVA with Tukey's correction was used; the adjusted *P*-values are shown. (*G*) Two-way ANOVA with Tukey's correction was used; the adjusted *P*-values are shown. BMDM, bone marrow-derived macrophage; HMDM, human monocyte-derived macrophage; TEPM, thioglycollate-elicited peritoneal macrophage; oxLDL, oxidized low-density lipoproteins; HFD, high-fat diet.

accumulation of NFATc3, the major NFAT isoform expressed in monocytes/macrophages, is reduced in macrophages from both humans and mice with atherosclerosis. NFATc3 deficiency in monocytes/macrophages promoted, whereas NFATc3 overexpression prevented, atherosclerotic plaque formation, and plaque instability. miR-204 is the direct target of NFATc3, which inhibits SR-A expression via canonical regulation and CD36 expression via non-canonical regulation, thus limiting the lipid uptake in macrophages and the progression of atherosclerosis. These findings suggest that macrophage NFATc3 functions as an inhibitor of atherogenesis. In this regard, our

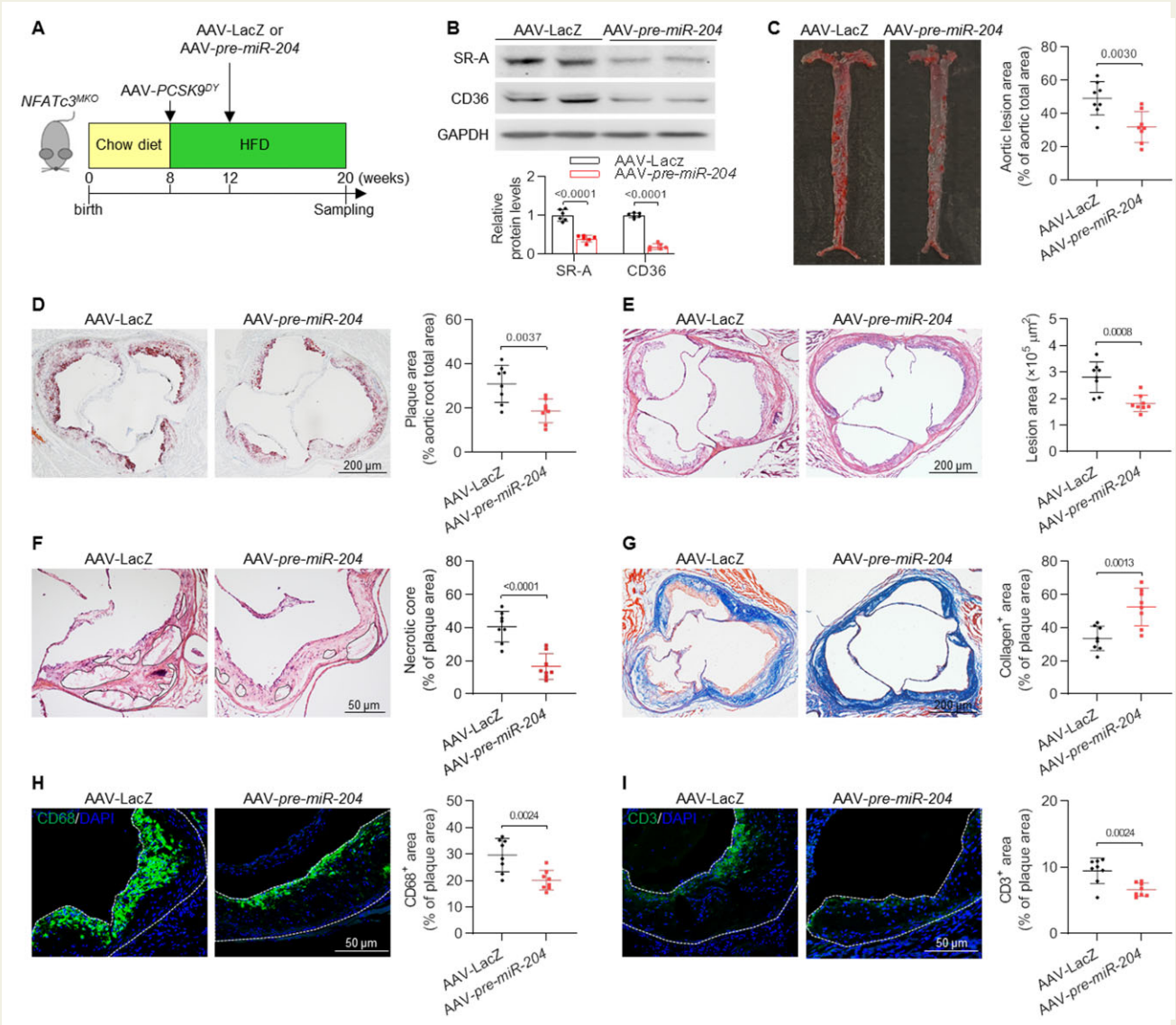

Figure 8 Restoration of miR-204 mitigates the deleterious effects of NFATc3 deficiency on atherosclerotic plaque development. (*A*) Schematic figure showing the experimental strategy for the adeno-associated virus administration, high-fat diet feeding, and subsequent analyses. (*B*) SR-A and CD36 protein levels in the thioglycollate-elicited peritoneal macrophages from the *NFATc3*^{MKO} mice administered adeno-associated viruses harbouring LacZ or the miR-204 precursor in a model of AAV-*PCSK9*^{DY}-induced atherosclerosis ($n = 6$ per group). Representative images and quantitative analysis of the Oil Red O-stained aortas (*C*) and aortic roots (*D*) of the mice from each group ($n = 8$ per group). Haematoxylin and eosin-stained sections of the aortic roots showing lesion formation (*E*) and necrotic core area (*F*) from each group ($n = 8$ per group). Representative images of the aortic root sections stained with Masson's trichrome stain (*G*), or immunostained for CD68 (*H*) or CD3 (*I*). The quantification results are shown on the right ($n = 8$ per group). Data are presented as the mean ± SD and comparisons were made using unpaired Student's *t*-test; the two-tailed *P*-values are shown. AAV, adeno-associated virus; HFD, high-fat diet.

results may explain why transplant patients receiving the immunosuppressive drugs cyclosporine A or FK506 are at a high risk of developing cardiovascular diseases, including atherosclerosis.

A sustained increase in $[Ca^{2+}]_i$ is known to induce nuclear translocation of NFATs through activation of the phosphatase calcineurin.[5] Our previous study has shown that oxLDL activates a sustained increase in $[Ca^{2+}]_i$.[17] Unexpectedly, the present data revealed that oxLDL treatment inhibited NFATc3 nuclear accumulation in macrophages. This result contrasts with the previous observations in vascular smooth muscle cells, where the hyperglycaemia- or hyperlipidaemia-induced elevation of $[Ca^{2+}]_i$ is an effective stimulus for NFATc3 nuclear translocation,[25] and in endothelial cells, where the tumor necrosis factor-α-induced increase in $[Ca^{2+}]_i$ is sufficient to increase NFATc4 nuclear accumulation.[26] The discrepancy may be due to the distinct sub-cellular distribution of NFATs in different types of cells. Similar to a previous study revealing that NFATc3 is confined to the nuclei of mouse BMDMs without stimulation,[27] we showed that NFATc3 is preferentially localized in the

nuclei of human PBMCs and mouse BMDMs; however, other studies have revealed that NFATc3 resides exclusively in the cytoplasm of unstimulated vascular smooth muscle cells or cardiomyocytes.[25,28] The nuclear localization of NFATc3 indicates that some molecules relay the cytoplasmic signals to the nucleus and thus contribute to the hyperlipidaemia-induced nuclear export of NFATc3. Indeed, several Ser/Thr protein kinases, including JNK, glycogen synthase kinase-3β, and protein kinase A, have been suggested to target NFATc3 and promote NFATc3 nuclear export.[18,19] Our recent work has demonstrated that oxLDL activates the calcineurin/ASK1/JNK signalling pathway in macrophages,[17] suggesting the involvement of JNK activation in oxLDL-induced NFATc3 nuclear export. This was confirmed in our present study, as blockade of JNK activation prevented the oxLDL-induced NFATc3 nuclear export.

Macrophage NFATc3 prevents atherosclerosis by blocking foam cell formation via inhibiting lipoprotein uptake, as evidenced by the decreased SR-A and CD36 expression. Strikingly, NFATc3 did not directly bind to the promoter of SR-A or CD36. By combining the results from two distinct gene expression platforms, we identified miR-204 as a high-confidence miRNA regulated by NFATc3. Moreover, NFATc3 binds to the miR-204 promoter and increased the miR-204 precursor levels. Previous studies have demonstrated that miR-204-5p levels are decreased during atherosclerosis and related metabolic diseases.[29–31] Herein, we found that the miR-204 precursor levels were also decreased in circulating PBMCs and plaque lesions of atherosclerosis patients. Furthermore, oxLDL suppressed the transcription of miR-204 by inhibiting the binding of NFATc3 to the miR-204 promoter, whereas NFATc3 restoration abrogated the oxLDL-induced inhibition of miR-204 transcription. More importantly, up-regulation of macrophage miR-204 reversed the NFATc3 deficiency-mediated enhancement of foam cell formation and atherosclerosis. The atheroprotective effects of miR-204 are consistent with those reported previously in endothelial cells, smooth muscle cells, and macrophages.[29,32,33] However, it has also been reported that miR-204-5p induces endothelial dysfunction associated with atherosclerosis.[31,34] The distribution of miR-204 upstream/downstream factors in diverse cell types, difference in extracellular stresses, and complexity of miRNA interaction may explain these variable results. Further studies are needed to address the precise functions of miR-204 in vascular cells. Collectively, these results identify NFATc3 as a key transcriptional modulator of oxLDL-mediated miR-204 down-regulation and suggest that the NFATc3/miR-204 axis plays an important role in atherosclerosis.

In addition to the canonical interactions between miRNA seed regions and targeted mRNA 3′-UTRs, increasing evidence has revealed an unexpected cell-type-specific localization of mature miRNAs in the nucleus, exerting additional and more widespread functions.[24,35,36] Herein, we are the first to demonstrate that miR-204-3p is specifically localized in the nucleus of macrophages. Moreover, we provided evidence that miR-204 regulates scavenger receptor expression via dual mechanisms, including the canonical post-transcriptional inhibition of SR-A via cytoplasmic miR-204-5p and the silencing of CD36 transcription via nuclear miR-204-3p. miRNAs harbouring any of the hexanucleotide sequences UGUGUU, ACUGUU, AGAGUU, AGUCUU, AGUGAU, AGUGUA, and AGNGUN are suggested to localize in the nucleus.[36] We observed the AGNGUN motif within the sequence of miR-204-3p. However, whether the nuclear localization of miR-204-3p is primarily determined by this motif remains to be assessed.

Notably, it has been previously shown that the nucleus-localized miRNAs participate in the epigenetic regulation via Ago2.[23,24] These observations differ from the traditional view of Ago2 being crucial for miRNA function by targeting mRNA 3′-UTRs in the cytoplasm to induce post-transcriptional gene silencing.[37,38] Herein, our data demonstrated that Ago2 could prevent the miR-204-3p-induced inhibition and promote the oxLDL-induced increase in CD36 transcription. Moreover, miR-204-3p and Ago2 bind to a same region within the CD36 promoter, indicating that they compete with each other for the binding to the CD36 promoter. The reduced enrichment of the histone modifications H3K27ac and H3K4me3 on the CD36 promoter further support the conclusion that miR-204-3p inhibits CD36 transcription. Thus, we proposed a working model for miR-204-3p in the nucleus in which nuclear miR-204-3p targets the CD36 promoter and decreases the Ago2 occupancy on the CD36 promoter, causing the effects of Ago2 on CD36 transcription to be suppressed.

Lipid-laden foam cells could induce cytokine secretion that recruits immune cells into the vascular wall and triggers inflammation, thereby promoting plaque formation.[1,3] We found that macrophage-specific NFATc3 up-regulation inhibited the recruitment of inflammatory cells into lesional vessels. Under *in vitro* conditions of atherosclerosis-like pathological stress, such as that induced by LPS/IFN-γ, NFATc3 induced lesional macrophages to shift to an anti-inflammatory state, thus limiting atherosclerosis progression. Intriguingly, our present data showed that the systemic levels of both IL-6 (pro-inflammatory) and IL-10 (anti-inflammatory) increased in *NFATc3*^{MTG} mice. This seemingly conflicting observation is similar to the results of a previous study, which reported that IL-10 synthesis and secretion are suppressed in IL-6-deficient mice, whereby the recruitment of inflammatory cells to the atherosclerotic plaques was enhanced,[39] suggesting that a balanced interplay between IL-6 and IL-10 may determine the perpetuation of atherogenesis. The anti-inflammatory role of macrophage NFATc3 differs from that reported in previous studies, which showed that NFATs target inflammation-related genes.[11,25,27] The inconsistency may be due to the counteracting effects of individual NFAT isoforms that compensate for the NFATc3 global deficiency (*NFATc3*$^{-/-}$) and play distinct roles in inflammation.[9,40] For example, the absence of NFATc3 is compensated by NFATc1 expression in the liver of *NFATc3*$^{-/-}$ mice,[40] which may influence the phenotype of macrophages, but this compensatory is unlikely to occur in *NFATc3*^{MKO} macrophages. Moreover, NFATc1 or NFATc3 knockdown has been shown to increase endothelial cell inflammation and monocyte adhesion, whereas NFATc2 or NFATc4 knockdown exerts opposite effects.[9] Thus, these findings, together with those of our study, highlight the importance of the isoform-specific manipulation of NFAT in specific settings.

In conclusion, we reported that macrophage NFATc3 exerts atheroprotective effects, which are primarily mediated by miR-204. Cytoplasmic miR-204-5p and nuclear miR-204-3p cooperatively inhibit the expression of scavenger receptors, leading to a stronger and more stable suppression of foam cell formation and atherosclerosis. Furthermore, our findings suggest that the NFATc3/miR-204 axis may represent a potential novel therapeutic target against atherosclerosis.

Supplementary material

Supplementary material is available at *European Heart Journal* online.

Acknowledgements

The authors acknowledged Dr Jia-Hua Fan and Dr Qiang-Sheng He of School of Public Health of Sun Yat-Sen University for their advice on statistics analysis.

Funding

This work was supported by the National Natural Science Foundation of China (81930106, 81525025, and 91739104 to J.-G.Z.; 81773723, 82073839, and 81603098 to S.-J.L.; 82001230 to Y.-H.T.; 81803519 to J.-Y.S.; 81903598 to X.-F.L.; and 81830013 to J.-S.O.); the National Key R&D Program of China (2017YFC0909302 to J.-G.Z.); the Science and Technology Program of Guangdong (2015TX01R159 to J.-G.Z.); the Natural Science Foundation of Guangdong (2019A1515011295 to R.-P.P. and 2015A030312009 to J.S.O.); and the High-level Health Team Foundation of Zhuhai (2018 to J.-G.Z.).

Conflict of interest: none declared.

Data availability

The data underlying this article will be shared on reasonable request to the corresponding author.

References

1. Lusis AJ. Atherosclerosis. *Nature* 2000;**407**:233–241.
2. Tousoulis D, Oikonomou E, Economou EK, Crea F, Kaski JC. Inflammatory cytokines in atherosclerosis: current therapeutic approaches. *Eur Heart J* 2016;**37**:1723–1732.
3. Li AC, Glass CK. The macrophage foam cell as a target for therapeutic intervention. *Nat Med* 2002;**8**:1235–1242.
4. Moore KJ, Tabas I. Macrophages in the pathogenesis of atherosclerosis. *Cell* 2011;**145**:341–355.
5. Crabtree GR, Olson EN. NFAT signaling: choreographing the social lives of cells. *Cell* 2002;**109**(Suppl):S67–S79.
6. Satterthwaite R, Aswad S, Sunga V, Shidban H, Bogaard T, Asai P, Khetan U, Akra I, Mendez RG, Mendez R. Incidence of new-onset hypercholesterolemia in renal transplant patients treated with FK506 or cyclosporine. *Transplantation* 1998;**65**:446–449.
7. Subramanian S, Trence DL. Immunosuppressive agents: effects on glucose and lipid metabolism. *Endocrinol Metab Clin North Am* 2007;**36**:891–905; vii.
8. Fric J, Zelante T, Wong AY, Mertes A, Yu HB, Ricciardi-Castagnoli P. NFAT control of innate immunity. *Blood* 2012;**120**:1380–1389.
9. Bretz CA, Savage SR, Capozzi ME, Suarez S, Penn JS. NFAT isoforms play distinct roles in TNFalpha-induced retinal leukostasis. *Sci Rep* 2015;**5**:14963.
10. Bushdid PB, Osinska H, Waclaw RR, Molkentin JD, Yutzey KE. NFATc3 and NFATc4 are required for cardiac development and mitochondrial function. *Circ Res* 2003;**92**:1305–1313.
11. Nilsson LM, Sun ZW, Nilsson J, Nordstrom I, Chen YW, Molkentin JD, Wide-Swensson D, Hellstrand P, Lydrup ML, Gomez MF. Novel blocker of NFAT activation inhibits IL-6 production in human myometrial arteries and reduces vascular smooth muscle cell proliferation. *Am J Physiol Cell Physiol* 2007;**292**:C1167–C1178.
12. Orr AW, Lee MY, Lemmon JA, Yurdagul A Jr, Gomez MF, Bortz PD, Wamhoff BR. Molecular mechanisms of collagen isotype-specific modulation of smooth muscle cell phenotype. *Arterioscler Thromb Vasc Biol* 2009;**29**:225–231.
13. Nilsson LM, Nilsson-Ohman J, Zetterqvist AV, Gomez MF. Nuclear factor of activated T-cells transcription factors in the vasculature: the good guys or the bad guys? *Curr Opin Lipidol* 2008;**19**:483–490.
14. Kobashigawa JA, Kasiske BL. Hyperlipidemia in solid organ transplantation. *Transplantation* 1997;**63**:331–338.
15. Tellides G, Pober JS. Interferon-gamma axis in graft arteriosclerosis. *Circ Res* 2007;**100**:622–632.
16. Malyszko J, Malyszko JS, Pawlak K, Mysliwiec M. The coagulo-lytic system and endothelial function in cyclosporine-treated kidney allograft recipients. *Transplantation* 1996;**62**:828–830.
17. Liang SJ, Zeng DY, Mai XY, Shang JY, Wu QQ, Yuan JN, Yu BX, Zhou P, Zhang FR, Liu YY, Lv XF, Liu J, Ou JS, Qian JS, Zhou JG. Inhibition of Orai1 store-operated calcium channel prevents foam cell formation and atherosclerosis. *Arterioscler Thromb Vasc Biol* 2016;**36**:618–628.
18. Chow CW, Rincon M, Cavanagh J, Dickens M, Davis RJ. Nuclear accumulation of nfat4 opposed by the JNK signal transduction pathway. *Science* 1997;**278**:1638–1641.
19. Gomez MF, Bosc LV, Stevenson AS, Wilkerson MK, Hill-Eubanks DC, Nelson MT. Constitutively elevated nuclear export activity opposes Ca2+-dependent NFATc3 nuclear accumulation in vascular smooth muscle: role of JNK2 and Crm-1. *J Biol Chem* 2003;**278**:46847–46853.
20. Huang EW, Liu CZ, Liang SJ, Zhang Z, Lv XF, Liu J, Zhou JG, Tang YB, Guan YY. Endophilin-A2-mediated increase in scavenger receptor expression contributes to macrophage-derived foam cell formation. *Atherosclerosis* 2016;**254**:133–141.
21. Wu QQ, Liu XY, Xiong LX, Shang JY, Mai XY, Pang RP, Su YX, Yu BX, Yuan JN, Yang C, Wang YL, Zhou P, Lv XF, Liu J, Zhou JG, Liang SJ. Reduction of intracellular chloride concentration promotes foam cell formation. *Circ J* 2016;**80**:1024–1033.
22. Maxwell KN, Breslow JL. Adenoviral-mediated expression of Pcsk9 in mice results in a low-density lipoprotein receptor knockout phenotype. *Proc Natl Acad Sci U S A* 2004;**101**:7100–7105.
23. Roberts TC. The microRNA biology of the mammalian nucleus. *Mol Ther Nucleic Acids* 2014;**3**:e188.
24. Li H, Fan J, Zhao Y, Zhang X, Dai B, Zhan J, Yin Z, Nie X, Fu XD, Chen C, Wang DW. Nuclear miR-320 mediates diabetes-induced cardiac dysfunction by activating transcription of fatty acid metabolic genes to cause lipotoxicity in the heart. *Circ Res* 2019;**125**:1106–1120.
25. Nilsson-Berglund LM, Zetterqvist AV, Nilsson-Ohman J, Sigvardsson M, González Bosc LV, Smith M-L, Salehi A, Agardh E, Fredrikson GN, Agardh C-D, Nilsson J, Wamhoff BR, Hultgårdh-Nilsson A, Gomez MF. Nuclear factor of activated T cells regulates osteopontin expression in arterial smooth muscle in response to diabetes-induced hyperglycemia. *Arterioscler Thromb Vasc Biol* 2010;**30**:218–224.
26. Yu BX, Yuan JN, Zhang FR, Liu YY, Zhang TT, Li K, Lv XF, Zhou JG, Huang LY, Shang JY, Liang SJ. Inhibition of Orai1-mediated Ca2+ entry limits endothelial cell inflammation by suppressing calcineurin-NFATc4 signaling pathway. *Biochem Biophys Res Commun* 2018;**495**:1864–1870.
27. Minematsu H, Shin MJ, Celil Aydemir AB, Kim KO, Nizami SA, Chung GJ, Lee FY. Nuclear presence of nuclear factor of activated t cells (NFAT) c3 and c4 is required for toll-like receptor-activated innate inflammatory response of monocytes/macrophages. *Cell Signal* 2011;**23**:1785–1793.
28. Liang Q, Bueno OF, Wilkins BJ, Kuan CY, Xia Y, Molkentin JD. c-Jun N-terminal kinases (JNK) antagonize cardiac growth through cross-talk with calcineurin-NFAT signaling. *EMBO J* 2003;**22**:5079–5089.
29. Wang N, Yuan Y, Sun S, Liu G. MicroRNA-204-5p participates in atherosclerosis via targeting MMP-9. *Open Med (Wars)* 2020;**15**:231–239.
30. Lin X, Xu F, Cui RR, Xiong D, Zhong JY, Zhu T, Li F, Wu F, Xie XB, Mao MZ, Liao XB, Yuan LQ. Arterial calcification is regulated via an miR-204/DNMT3A regulatory circuit both in vitro and in female mice. *Endocrinology* 2018;**159**:2905–2916.
31. Wang R, Ding YD, Gao W, Pei YQ, Yang JX, Zhao YX, Liu XL, Shen H, Zhang S, Yu L, Ge HL. Serum microRNA-204 levels are associated with long-term cardiovascular disease risk based on the Framingham risk score in patients with type 2 diabetes: results from an observational study. *J Geriatr Cardiol* 2020;**17**:330–337.
32. Lu G, Tian P, Zhu Y, Zuo X, Li X. LncRNA XIST knockdown ameliorates oxidative low-density lipoprotein-induced endothelial cells injury by targeting miR-204-5p/TLR4. *J Biosci* 2020;**45**:52.
33. Yan L, Liu Z, Yin H, Guo Z, Luo Q. Silencing of MEG3 inhibited ox-LDL-induced inflammation and apoptosis in macrophages via modulation of the MEG3/miR-204/CDKN2A regulatory axis. *Cell Biol Int* 2019;**43**:409–420.
34. Vikram A, Kim YR, Kumar S, Li Q, Kassan M, Jacobs JS, Irani K. Vascular microRNA-204 is remotely governed by the microbiome and impairs endothelium-dependent vasorelaxation by downregulating sirtuin1. *Nat Commun* 2016;**7**:12565.
35. Das S, Ferlito M, Kent OA, Fox-Talbot K, Wang R, Liu D, Raghavachari N, Yang Y, Wheelan SJ, Murphy E, Steenbergen C. Nuclear miRNA regulates the mitochondrial genome in the heart. *Circ Res* 2012;**110**:1596–1603.
36. Mendell JT, Hwang HW, Wentzel EA. Nucleotide motifs providing localization elements and methods of use. World Intellectual Property Organization 2007; WO 2007/149521 A2.
37. Hansen TB, Wiklund ED, Bramsen JB, Villadsen SB, Statham AL, Clark SJ, Kjems J. miRNA-dependent gene silencing involving Ago2-mediated cleavage of a circular antisense RNA. *EMBO J* 2011;**30**:4414–4422.

38. Kim DH, Saetrom P, Snove O Jr, Rossi JJ. MicroRNA-directed transcriptional gene silencing in mammalian cells. *Proc Natl Acad Sci U S A* 2008;**105**: 16230–16235.
39. Schieffer B, Selle T, Hilfiker A, Hilfiker-Kleiner D, Grote K, Tietge UJ, Trautwein C, Luchtefeld M, Schmittkamp C, Heeneman S, Daemen MJ, Drexler H. Impact of interleukin-6 on plaque development and morphology in experimental atherosclerosis. *Circulation* 2004;**110**:3493–3500.
40. Pierre KB, Jones CM, Pierce JM, Nicoud IB, Earl TM, Chari RS. NFAT4 deficiency results in incomplete liver regeneration following partial hepatectomy. *J Surg Res* 2009;**154**:226–233.